RESEARCH ARTICLE

Quantifying the Solution Structure of Metal Nanoclusters Using Small-Angle Neutron Scattering

Xindi Liu,[a] Huayan Yang,*[b] Yuxiang Chen,[c] Ye Yang,[d] Lionel Porcar,[e] Aurel Radulescu,[f] Stefan Guldin,[d] Rongchao Jin,[c] Francesco Stellacci,[g] Zhi Luo*[a]

[a] Guangdong Provincial Key Laboratory of Advanced Biomaterials, Department of Biomedical Engineering, Southern University of Science and Technology, Shenzhen 518055, Guangdong, China. E-mail: luoz@sustech.edu.cn.
[b] Department of Medicine, Shenzhen University, Shenzhen 518055, Guangdong, China. E-mail: yanghuayan@szu.edu.cn.
[c] Department of Chemistry, Carnegie Mellon University, Pittsburgh, Pennsylvania 15213, United States.
[d] Department of Chemical Engineering, University College London, WC1E 7JE London, United Kingdom.
[e] Institut Laue-Langevin, BP 156, F38042 Grenoble CEDEX 9, France.
[f] Jülich Center for Neutron Science, JCNS at Heinz Maier-Leibnitz Zentrum, Forschungszentrum Jülich GmbH, 85747 Garching, Germany.
[g] Institute of Materials, École Polytechnique Fédérale de Lausanne, 1015 Lausanne, Switzerland.

Supporting information for this article is given via a link at the end of the document.

Abstract: Metal nanoclusters are a unique class of synthetic material, as their crystal structures can be resolved using X-ray diffraction, and their chemical formula can be precisely calculated from mass spectroscopy. However, the complete structure determination by these two techniques is often a challenging task. Here, we utilize small angle neutron scattering (SANS) to directly quantify the key structure parameters of a series of silver and gold nanoclusters in solution, which correlates well to their crystallographic structures. Besides, SANS also allows the quantification of the counterions layer surrounding charged nanoclusters in solution. Furthermore, when combining with X-ray scattering, it is possible to estimate the molecular weight of both the metal core and the ligand shell of nanoclusters. This work offers an alternative characterization tool for nanoclusters without the requirement of crystallization or gas phase ionization.

Introduction

Metal nanoclusters (NCs) are an emerging type of nanomaterial with unique optical, magnetic, and catalytic properties.[1] NCs are atomically monodisperse, i.e., they can be represented by definite chemical formulas and their structures can be resolved by X-ray crystallography.[2] The characterization of NCs has revealed different types of metal-organic coordination architectures and uncovered the emergence of surface plasmonic resonance.[3] Understanding the structure-property relationships of NCs is also of great importance for their potential applications in various fields.[2] For example, the core size and ligand shell arrangement are critical for the in vivo fate of the NCs when acting as drug carriers or imaging agents.[4] Similarly, the high surface-to-volume ratio of the NCs results in efficient atomic utilization, which is of great promise for the development of novel catalysts.[5–12]

Due to their ultrasmall sizes and atomic-precision nature, the characterization of NCs often follows that of proteins rather than colloidal nanoparticles, with the latter typically relying on techniques such as electron microscopy (EM), dynamic light scattering (DLS) and SAXS.[13–15] In contrast, the atomic structure of NCs is resolved using single crystal X-ray diffraction (XRD) and their exact chemical composition is determined by mass spectrometry,[16–25] which is similar to the giant polyoxometalate molecules formed covalently by connecting transition metals and oxide polyhedrals.[26–28] Although the precise characteristics of many NCs have already been resolved, there are clear limitations of these two techniques. Specifically, obtaining high quality single crystals for XRD is often a formidable challenge due to the size of the NCs as well as the flexibility of the organic ligands, which increases the disorder in crystals.[29] For mass spectrometry, the ionization of the samples, especially for larger NCs, tends to be difficult, and ligand loss may also occur.[30] Moreover, so far, there are only few techniques, such as nuclear magnetic resonance (NMR) and analytical ultracentrifugation (AUC), that could be used to directly study the properties of NCs in their native state in solution.[31] For instance, several studies have utilized DOSY-NMR and AUC to determine their hydrodynamic size and the heterogeneity of distinct NC sizes in the ensemble.[32,33] However, the information extracted from these methods is limited. Another potentially informative technique for NC solutions is the multi-dimensional NMR techniques. Unfortunately, the heterogeneous and dynamic chemical environment complicates the interpretation of the spectra, making it often rather a complementary method only.[34]

Small-angle neutron scattering (SANS) is a powerful technique to study the structural arrangement of multicomponent materials at the nanoscale.[35] Thanks to its sensitivity to isotope labeling, especially deuteration, the scattering contrasts of different constituents can be fine-tuned making it possible to highlight the morphology of the organic ligand shell even in the presence of the heavy metal core.[36,37] For instance, using a core-shell model, the accurate structure parameters such as the core size and distribution, the thickness as well as the solvation degree of the ligands for various types of nanoparticles can be extracted.[38,39] Using selective deuteration and solvent contrast variation techniques, it is possible to reconstruct the self-assembled structures of binary ligand mixtures obtained by phase separation on the nanoparticle surfaces.[35,40–44] Besides model-based analytical methods, small angle scattering could directly quantify several global parameters, such as the radius of gyration (R_g), Porod volume (V_p), surface-to-volume ratio, compactness and correlation length (l_c). Recently, by defining a new scattering invariant, i.e., volume of correlation (V_c), Rambo et al. developed

a method to accurately determine the molecular mass of proteins or RNA ranging from 10 to 1,000 kilodaltons.[45]

Although both SANS and small angle X-ray scattering (SAXS) are typically regarded as low-resolution techniques that cannot access atomic scale information, the structural parameters retrieved from scattering patterns have been reported to be highly accurate. For proteins, the heterogeneous hydration layer, whose thickness is typically in the range of a few Ångström, could be precisely evaluated using SANS.[46,47] The core-shell model based analytical fitting of the SANS data from nanoparticles can also provide dimensional parameters with Ångström accuracy[48] and distinguish ligand shell structures that differ by only a few molecules.[35] Utilizing SAXS and Monte Carlo type fitting, Dass and co-workers investigated the metal core structure of several NCs, such as Au_{329} and $Au_{\sim 940}$.[18,49] However, due to the low contrast in X-ray scattering, the ligand shell structures of those NCs were not accessible. So far, there are no reports that explore the application of SANS in characterizing both ligand shell and metal core arrangement of NCs in a holistic fashion.

Here, we report a systematic study on the neutron scattering of atomically precise NCs in solution. Adopting an ellipsoid core-shell model, we successfully fitted the SANS data of a series of silver and gold NCs, including Ag_{16}, Ag_{38}, Ag_{44}, Ag_{63}, Ag_{136}, Ag_{374} as well as Au_{38}, Au_{104}, Au_{144}. Both the size and geometry parameters calculated from SANS were found to be consistent with the crystallographic results for these NCs. Interestingly, for some NCs that carry multiple intrinsic charges, such as Ag_{44}, the overall diameter appeared significantly larger than other NCs with similar numbers of metal atoms. We attribute this observation to the presence of counter-ions in solution. Therefore, SANS could not only provide quantitative structure information without the need of crystallization but also allow for the examination of the surrounding molecules of NCs in solution. Furthermore, using the contrast variation SANS, we also established a power-law relationship between the scattering invariants and the molecular weights of the NCs demonstrating the potential of SANS to serve as a supplementary technique for mass spectrometry.

Results and Discussion

To date, most of the NCs discovered are composed of less than ~1000 metal atoms and ~200 organic ligands, which corresponds to an overall size of less than 5 nm for the majority of NCs.[49] Therefore, all the SANS measurements in this work were performed with a short sample to detector distance (1.2 m) recording a q range of 0.04 to 0.8 $Å^{-1}$, corresponding to 7 Å to 150 Å in real space. Thus, the scattering patterns contain the full form factor information and cover the entire Guinier region. As the scattering intensity at such high q angles is typically quite low, the SANS measurements in this work were performed using solvents with high deuteration contents to minimize the incoherent scattering background. Depending on the core size and the ligand chemical structure of the NCs, different deuterated solvents, such as d-toluene, d-N,N-dimethylformamide (d-DMF), d-chloroform ($CDCl_3$), d-dichloromethane (d-DCM), were chosen to ensure high solubility under good solvent conditions and minimize the inter-particle interactions. The sample concentration was approximately 10 mg/mL corresponding to a volume fraction of NCs in solution of less than 0.1%. Due to the good solubility and low volume fraction, the NC samples were found to be in the non-interacting regime and the structure factor contribution to the scattering intensity could therefore be neglected. This was confirmed with SAXS measurements characterized by a flat and featureless pattern at the low scattering angles, as shown in Figure S1.

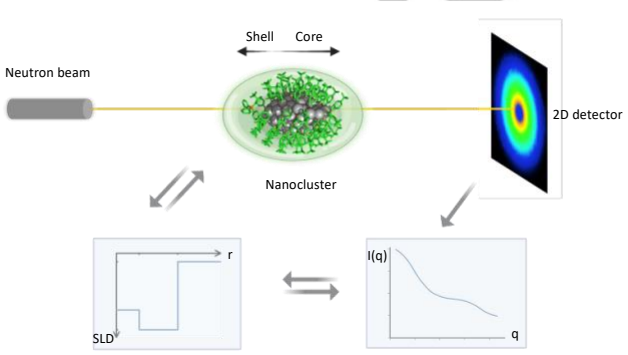

Figure 1. Schematic illustration of SANS measurement on NCs. One dimensional scattering pattern is reduced from the solution scattering profile of NCs. A core-shell model with three different stages of SLD contrasts (core, shell, and solvent) is used to interpret the data.

While most of the NC structures are isotropic, a number of NCs were found to be non-spherical. For example, the Au_{38} is known for its rod-like metal core[21], and the Ag_{374} and Ag_{136} feature an oblate disk-like structure.[25] Therefore, instead of using simple spherical models to fit the scattering curve as in the case of colloidal nanoparticles, a core-shell ellipsoid model was found to be a better representation of the NC structures (Figure 1).[50] The fitting analysis was performed multiple times using both SASview (http://www.sasview.org/) and SASfit software[51] to cross validate the calculated results. The scattering length densities (SLDs) of the metal core, ligand shell as well as the deuterated solvents were calculated (Table S1) and given as the fixed parameters during the fitting. As shown in Eq. 1, several important structure parameters are extracted from the ellipsoid model fitting to describe the overall structure of the NCs, i.e., the equatorial radius (R_e), the polar radius (R_p), and the thickness of the shell (t_{shell}). A parameter x_{core} was defined by the ratio of the R_p and R_e acting as a measure of the axial ratio of the metal core for the NCs.[36,50]

$$P(q,\alpha)=\frac{scale}{V}\left[f(q,\ R_e,\ R_e\cdot x_{core}\ ,\ \alpha)+f(q,\ R_e,+t_{shell},\ R_e\cdot x_{core}\ +t_{shell}\cdot x_{shell,}\ \alpha)\right]^2 +background \quad \text{Eq. 1}$$

where,

$$f(q,R_e,R_p,\alpha)=\frac{3\Delta\rho V\left(\sin\left[qr\left(R_p,R_e,\alpha\right)\right]-\cos\left[qr\left(R_p,R_e,\alpha\right)\right]\right)}{\left[qr\left(R_p,R_e,\alpha\right)\right]^3}$$

and,

$$r\left(R_e,R_p,\alpha\right)=\left[R_e^2(\sin\alpha)^2+R_p^2(\cos\alpha)^2\right]^{1/2}$$

A series of silver NCs with different sizes including, Ag_{16}, Ag_{38}, Ag_{44}, Ag_{63}, Ag_{136}, and Ag_{374}, were synthesized as previously reported.[20,23–25] For all the NCs, a measurement time of 30 min was found to be sufficient to collect SANS curves with an acceptable signal-to-noise ratio. As shown in Figure 2, the scattering curves of Ag_{374} and Ag_{136} present at high q angles the oscillations typical of nanoparticles, given that their sizes are

close to that of conventional colloids. In comparison, the rest of the NCs demonstrate much less defined oscillation patterns due to their smaller sizes. The structure parameters extracted from the core-shell ellipsoid model fitting are summarized in Table 1. The core radii were found to be 5.2 ± 0.1 Å, 5.6 ± 0.3 Å, 6.4 ± 4.5 Å, 8.3 ± 0.1 Å, 11.5 ± 0.3 Å, and 15.1 ± 0.2 Å for Ag_{16}, Ag_{38}, Ag_{44}, Ag_{63}, Ag_{136}, and Ag_{374}, respectively. Such values agree well with what were measured from the crystal structures of these NCs.[20,23–25] Moreover, the x_{core} from the fitting results for these six NCs were 0.8, 1.0, 0.9, 0.7, 0.7, and 0.7 for Ag_{16}, Ag_{38}, Ag_{44}, Ag_{63}, Ag_{136}, and Ag_{374}, respectively. As suggested by the crystal structures, while the shapes of Ag_{16} and Ag_{44} may be approximated as spherical, Ag_{38} displays a half-cube shape and Ag_{63} is nearly cubic. The remaining NCs, Ag_{136}, and Ag_{374}, are disk-like and deviate further from a perfect spherical shape.

As the NCs were not protected by the same ligands, different values for the t_{shell} were also observed from the fitting. For Ag_{38} and Ag_{63} with the same main component of the ligands, 3,4-difluorobenzenethiol ($SC_6H_3F_2$), the t_{shell} was found to be 1.9 ± 0.3 Å and 6.5 ± 0.1 Å, respectively. A shell thickness (4.6 ± 1.2 Å) was found for Ag_{16}, which is protected by a mixture of $SC_6H_3F_2$ and 1,2-bis(diphenylphosphino)ethane (DPPE). In comparison, the 4-tert-butylbenzenethiolate (4-*t*BuPhSH-) protected Ag_{136} and Ag_{374} feature a shell thickness of 8.9 ± 0.4 Å and 7.0 ± 0.3 Å, respectively. All the differences in shell thickness calculated from SANS fitting were confirmed by crystal structures. Similar capability in resolving the small structure variations were reported in the evaluation of the hydration profile of proteins using SANS.[46] This result proves again the accuracy of SANS analysis and its Å-scale sensitivity in distinguishing small structure differences.

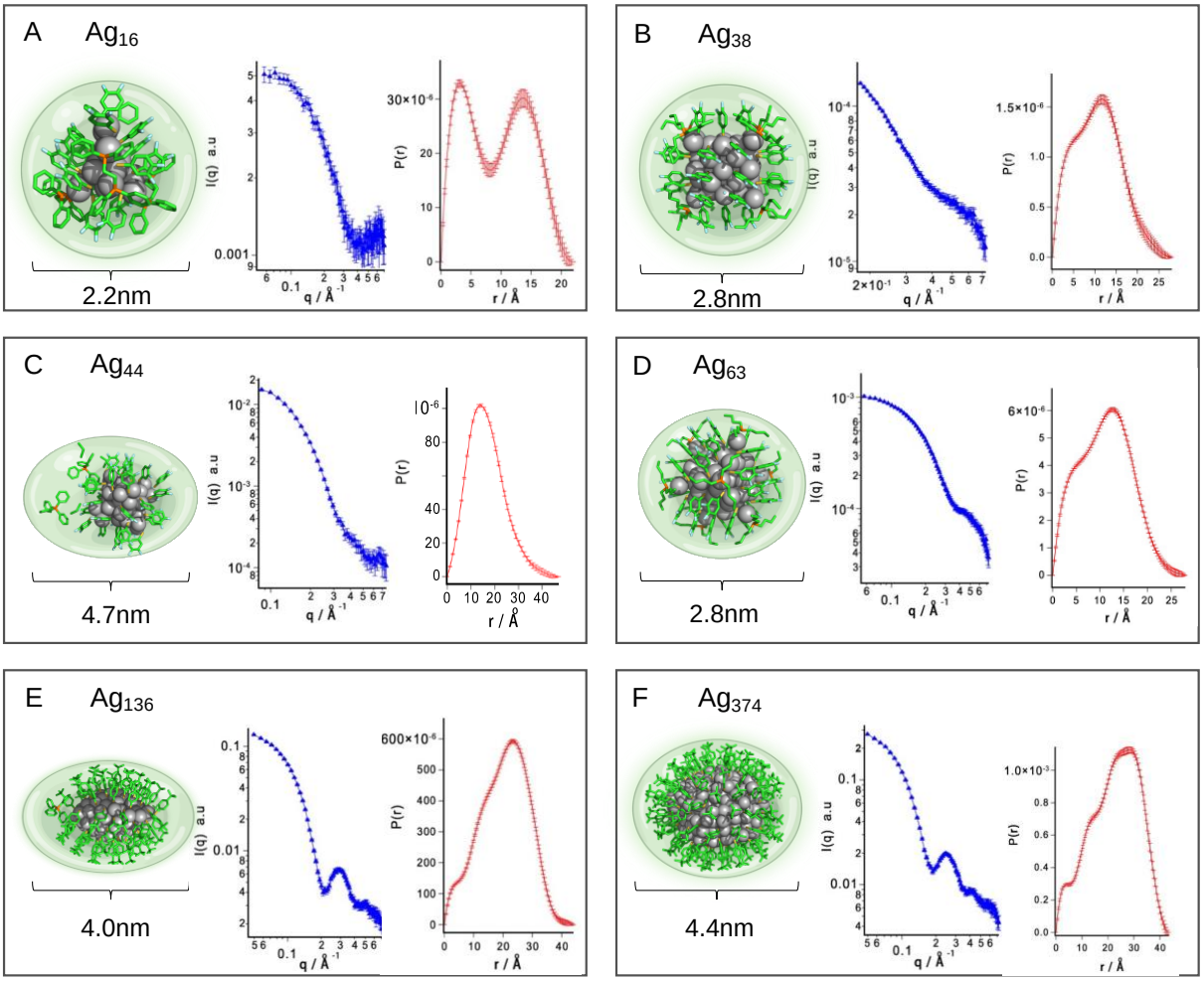

Figure 2. Comparison between the single crystal structures of Ag NCs, their SANS data and corresponding P(r) analysis for (A) $Ag_{16}(DPPE)_4(SC_6H_3F_2)_{14}$, (B) $Ag_{38}(SPhF_2)_{26}(P^nBu_3)_8$, (C) $Ag_{44}(SPhF_2)_{30}$, (D) $Ag_{63}(SPhF_2)_{36}(P^nBu_3)_8$, (E) $Ag_{136}(SPht Bu)_{64}Cl_3PPh_4$, and (F) $Ag_{374}(SPht Bu)_{113}Br_2Cl_2$. For $Ag_{38}(SPhF_2)_{26}(P^nBu_3)_8$, the SANS data was truncated at low q region, due to the poor solubility and slight aggregation of this nanocluster in solution. The single crystal structure plots were reproduced from data retrieved by the Cambridge Crystallographic Data Centre (CCDC) under deposition numbers CCDC-916463 for Ag_{16}, CCDC-1530606 for Ag_{38}, CCDC-953878 for Ag_{44}, CCDC-1530604 for Ag_{63}, CCDC-1496142 for Ag_{136}, CCDC-1496141 for Ag_{374}.[20,23–25] Grey spheres represent silver atoms while green sticks are organic molecules. The SANS data for Ag_{374}, Ag_{136} and Ag_{16} were collected using $CDCl_3$ as solvent and for the Ag_{44} and Ag_{16} the solvents were d-DMF and d-DCM, respectively.

The only significant deviation of the fitting results from crystal structures was the shell thickness of Ag_{44} (11.6 ± 4.6 Å from SANS compared to 6.9 Å in crystal). Also, to further explain the relatively larger error in the fitting of Ag_{44}, CRYSON fitting was performed on the SANS data of Ag_{44}.[46] An obvious inconsistency with its crystal structure and SANS data was observed. We tentatively attribute such a difference to the presence of counter-ions in the solution. In fact, among all these silver NCs, Ag_{44} is the only one that carries four negative charges. During its synthesis, a positively charged molecule, tetraphenylphosphonium (TPP), was added and acted as the counter-ion. Therefore, the ~5 Å difference represents the space occupied by the TPP counter-ions in solution, which indeed agrees well with the crystal structure of TPP. Therefore, the core-shell ellipsoid model may not be the most precise model to describe the nanoclusters with counterion layers. Noteworthily, there are several reports that emphasize on the effects of counterions on the properties of NCs. In colloid systems, the size of counterions is orders of magnitude smaller than that of the particles and hence they are often regarded as point charges.[52] However, in the case of NCs, the dimension of counterions and particles becomes comparable and could not be neglected, as they play a decisive role in many unique interfacial properties of the NCs. For example, Yao *et al.* reported that the geometry of Ag_{44} NCs supracrystals can be varied by altering the concentration and types of the counter-ions.[53] Zheng and co-workers reported that the counter-ions of NCs not only act as stabilizing agents for charged NCs but could also promote the crystallization of chiral NCs.[54] Therefore, the capability of SANS in determining counter-ion layer structures may contribute to the future application of NCs in solution phase.

Table 1. Fitting parameters for different nanoclusters NCs employing a core-shell ellipsoid model as described in Eq 1. R_e and t_{shell} represent for the radius of metal core and the thickness of the ligand shell, and x_{core} is the ratio of thickness of shell at pole to that at equator.

	D_{max} (Å)		R_e (Å)		t_{shell} (Å)		x_{core}	
	P(r)	Crystal	Fitting	Crystal	Fitting	Crystal	Fitting	Crystal
Ag_{16}	22.0	21.9	5.2	5.8	4.6	6.1	0.8	1.0
Ag_{38}	28.0	27.3	5.6	7.2	1.9	5.9	1.0	0.9
Ag_{44}	47.0	32.0	6.4	8.2	11.6	6.9	0.9	1.0
Ag_{63}	28.0	26.8	8.3	8.3	6.5	5.2	0.7	0.8
Ag_{136}	44.0	40.5	11.5	12.0	8.9	7.1	0.7	0.5
Ag_{374}	43.0	42.0	15.1	15.7	7.0	7.5	0.7	0.7
Au_{38}	28.0	27.3	4.6	4.8	9.3	7.9	0.9	0.8
Au_{104}	32.0	*	9.6	*	8.8	*	0.8	*
Au_{144}	35.0	28.1	9.4	8.7	6.9	6.1	1.2	0.9

* The crystal structure of Au_{104} has not been reported yet.

Besides the analytical fitting, some global properties can be directly extracted from SANS curves. As shown in Figure 2, the pair distance distribution function, P(r), was calculated using GNOM package.[55] A typical bell shape was observed with the P(r) for Ag_{38}, Ag_{44} and Ag_{63}, confirming again the spherical structure of these NCs. A shoulder in P(r) at the small distance range can be observed for Ag_{136} and Ag_{374}, it qualitatively agrees with their disk-like shape feature. Similarly, the P(r) of Ag_{16} is characterized by a two-peak profile, which is typical for rod-like structure.[24] The D_{max} calculated from P(r) represents the largest pair distance in the scattering object, which equals to the outmost diameter of the NCs including the ligand shell. The determination of the overall sizes of NCs from the D_{max} value was performed and quantitatively compared to that measured from the crystal structures (Table 1). The deviation of D_{max} values from SANS was found to be less than 10 % representing only a few Å discrepancy for most NCs. Again, in the case of Ag_{44}, the D_{max} values were significantly larger than the sole core-shell size of the NCs, with 4.4 nm and 3.2 nm, respectively. Accordingly, this shows that the counter-ion layer accounts for 0.8 nm thickness in solution.

We also performed SANS analysis on three different sizes of gold NCs, i.e., Au_{38}, Au_{104}, and Au_{144}. As shown in Figure 3, the D_{max} were found to be 3.5 nm, 3.2 nm, and 2.8 nm, respectively. The fitting parameters of the core-shell ellipsoid model can be referred to Table 1. For gold NCs with known crystal structures, i.e., Au_{38} and Au_{144}, quantitative agreement between the fitting results and the single crystal structures was achieved. Specifically, the equatorial radius R_e of metal core for Au_{38} and Au_{144} are 4.6 ± 6.1 Å and 9.4 ± 0.6 Å, respectively, with corresponding shell thicknesses t_{shell} of 9.3 ± 6.2 Å and 6.9 ± 1.0 Å. It should be noted that the single crystal structure of Au_{104} has not been reported yet. According to our fitting results, the suggested global shape of Au_{104} appears to be an ellipsoid with an x_{core} value of 0.8. The calculated Au_{104} crystal structure composes of a metal core of 9.6 ± 0.7 Å and the ligand shell of 8.8 ± 0.7 Å. Essentially, such prediction is close to the structure of its neighbor Au_{103}.[56] The result demonstrated the advantage of SANS in providing structural information without the need for crystallization. Hopefully, such data could act as a reference for future experimental and theoretical analysis of Au_{104}.

Moreover, we explored the possibility of combining SAXS and SANS in determining the molecular weight (M_W) of NCs. According to Rambo et. al., a new scattering invariant, the volume of correlation (V_c) can be utilized to accurately evaluate the M_W of biomacromolecules, such as proteins and RNAs.[45] As described

in Eq 2, V_c is independent of the concentration of the samples and can avoid systematic errors of concentration measurements in the conventional Guinier methods. They also defined Q_R which is the ratio of the squared of V_c to R_g with a unit of Å^3.[45] Explicitly, l_c is per self-correlation length and V_P is particle's volume. It has been found that Q_R follows a power-law with the mass of a protein, which is shown in Eq 3. Using these invariants in SAXS, a previous study has reported less than 4% error in the evaluation of the mass of proteins.[45]

$$V_c = \frac{I(0)}{\int qI(q)dq} = \frac{cV_P^2(\Delta\rho)^2}{cV_P(\Delta\rho)^2 2\pi l_c} = \frac{V_P}{2\pi l_c} \quad \text{Eq.2}$$

$$Q_R = \left(\frac{V_c^2}{R_g}\right) \quad \text{Eq.3}$$

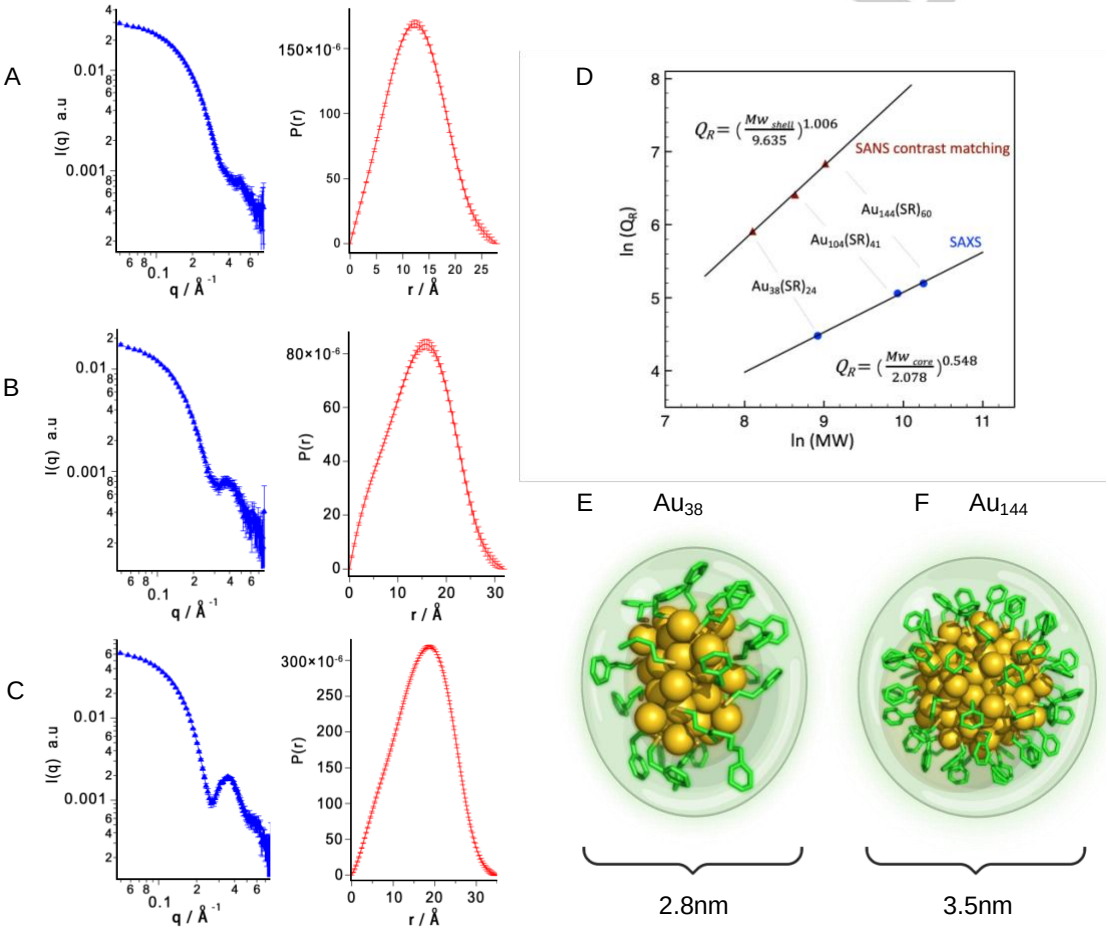

Figure 3. SANS data and P(r) plots of Au_{38}(A), Au_{104}(B) and Au_{144}(C) NCs. All SANS data was collected using deuterated toluene as solvent. The Power-law relationship (D) between the Q_R and the core and ligand shell mass of the nanoclusters was calculated using the ScÅtter software.[57–59] The differences of the exponent coefficient originates from different contrast conditions. The exponent for the gold core was calculated from SAXS data while for the case of ligand shell, it was determined from contrast matching SANS data. The single crystal structures of Au_{38} (E) and Au_{144} (F) were reproduced from the reference.[21,29] Yellow spheres are the gold core and green sticks are the organic ligand shell. The single crystal structure plots were reproduced from data retrieved by the Cambridge Crystallographic Data Centre (CCDC) under deposition numbers CCDC-785582 for Au_{38}, CCDC-1873120 for Au_{144}.

Here, to calculate the M_W of the metal core and the ligand shell separately, we performed both SAXS and contrast variation SANS measurements on three gold NCs. A mixture of deuterated (79 %) and non-deuterated (21 %) toluene was used as solvent, which exhibits a SLD that matches the contrast of the gold core. Therefore, the scattering intensity solely comes from the ligand shell. In comparison, in SAXS measurements, the contrast of the organic shell is close to that of the solvent and thus the scattering patterns only contain information from the gold core. Consequently, a separate power-law relationship between the Q_R and molecular weight for both the core and ligand shell of NCs could be established as presented in Figure 3 with the molecular weight of the metal core and the ligands shell being calculated respectively (Figure S11). Similar to the case of proteins, a highly linear trend of the power-law relationship was observed for the NCs, confirming the accuracy of the M_W analysis using SANS and SAXS. It should be noted that for both SANS and SAXS, a deviation of less 10% between the real M_W and the calculated values was observed. For the analysis of the metal core, the deviation was 1.7%, 3.5% and 4.9% for Au_{38}, Au_{104} and Au_{144}

respectively, which corresponds to a discrepancy of 1- 7 atoms, which further proves the accuracy of SANS and SAXS analysis on nanoclusters.

As in the molecular weight calculation with SAXS, a deviation of <10% was observed with SANS analysis on the M_W of the ligand shell. Considering the number of ligands on nanoclusters being in the order of 10-100, such deviation means that SANS could achieve molecular precise information (1-10 molecules). In principle, one could also extract the M_W using SANS through the deuteration of ligands to match the contrast to the solvent. However, such deuterated thiolated ligands are not easily available. Therefore, we believe that the combination of SAXS and SANS offers the most convenient way to get the information on both the metal core and ligand shell.

Furthermore, we have performed the fitting of Au_{38} and Au_{144} using the CRYSOL package.[60] As shown in Fig S12 and Fig S13, the CRYSOL calculation of Au_{144} from its crystal structure reached good consistency with the experimental SAXS data with a χ^2 value of 7.0 x 10^{-7}. The quality of the fitting again proves the validity of data analysis in this work. For Au38, a χ^2 of 4.8 x 10^{-7} was obtained with CRYSOL fitting. The higher inconsistency may be due to the ultrasmall size of Au38 and the effect of surface ligands that contributes to the scattering.

Conclusion

In conclusion, we have demonstrated the capabilities of SANS in the characterization of NCs in solution. Although the dimension of NCs is small, accurate core and ligand shell structure information can be readily evaluated by this method. Different from solid state analyses such as X-ray crystallography, SANS measurements could capture the presence of counter-ion layers in solution. The knowledge on the presence of counter-ions is important for understanding the electronic structure and interfacial properties of NCs. Additionally, for NCs whose crystallographic data is unavailable due to difficulties in crystallization, or when the M_W is challenging to be determined, the contrast-matching SANS method and SAXS offer a reliable way to estimate the structural parameters. For structure biology and biophysics, SANS and SAXS has contributed greatly to the study of biological samples in their native solution state. Compared with conventional colloidal nanoparticles, atomically precise NCs have much in common with proteins. We therefore envision that solution-based SANS will obtain growing attention in the field of NCs for the analysis of structural properties and interactions in solution and thus hold great promise as a unique characterization tool for NCs.

Acknowledgements

Financial support from Guangdong Provincial Key Laboratory of Advanced Biomaterials (2022B1212010003) is acknowledged. This work benefited from the use of the SasView application, originally developed under NSF award DMR-0520547. SasView contains code developed with funding from the European Union's Horizon 2020 research and innovation program under the SINE2020 project, grant agreement No 654000.

Keywords: core-shell structures • counter-ions • nanoclusters • neutron scattering • structure elucidation

[1] R. Jin, *Nanoscale* **2010**, *2*, 343–362.
[2] R. Jin, C. Zeng, M. Zhou, Y. Chen, *Chem. Rev.* **2016**, *116*, 10346–10413.
[3] H. Qian, Y. Zhu, R. Jin, *Proc. Natl. Acad. Sci.* **2012**, *109*, 696–700.
[4] G. Li, R. Jin, *Acc. Chem. Res.* **2013**, *46*, 1749–1758.
[5] N. Kaur, R. N. Aditya, A. Singh, T.-R. Kuo, *Nanoscale Res. Lett.* **2018**, *13*, 302.
[6] G. Schmid, M. Bäumle, M. Geerkens, I. Heim, C. Osemann, T. Sawitowski, *Chem. Soc. Rev.* **1999**, *28*, 179–185.
[7] Z. Luo, K. Zheng, J. Xie, *Chem Commun* **2014**, *50*, 5143–5155.
[8] X.-R. Song, N. Goswami, H.-H. Yang, J. Xie, *The Analyst* **2016**, *141*, 3126–3140.
[9] Y. Zheng, J. Wu, H. Jiang, X. Wang, *Coord. Chem. Rev.* **2021**, *431*, 213689.
[10] Y. Genji Srinivasulu, Q. Yao, N. Goswami, J. Xie, *Mater. Horiz.* **2020**, *7*, 2596–2618.
[11] Y. Tao, M. Li, J. Ren, X. Qu, *Chem. Soc. Rev.* **2015**, *44*, 8636–8663.
[12] L. Shang, S. Dong, G. U. Nienhaus, *Nano Today* **2011**, *6*, 401–418.
[13] H. Qian, M. Zhu, Z. Wu, R. Jin, *Acc. Chem. Res.* **2012**, *45*, 1470–1479.
[14] Y. Yang, S. Liao, Z. Luo, R. Qi, N. Mac Fhionnlaoich, F. Stellacci, S. Guldin, *Nanoscale* **2020**, *12*, 12007–12013.
[15] R. Jin, S. Zhao, Y. Xing, R. Jin, *CrystEngComm* **2016**, *18*, 3996–4005.
[16] A. Das, T. Li, G. Li, K. Nobusada, C. Zeng, N. L. Rosi, R. Jin, *Nanoscale* **2014**, *6*, 6458.
[17] P. D. Jadzinsky, G. Calero, C. J. Ackerson, D. A. Bushnell, R. D. Kornberg, *Science* **2007**, *318*, 430–433.
[18] C. Kumara, X. Zuo, J. Ilavsky, K. W. Chapman, D. A. Cullen, A. Dass, *J. Am. Chem. Soc.* **2014**, *136*, 7410–7417.
[19] M. Zhu, C. M. Aikens, F. J. Hollander, G. C. Schatz, R. Jin, *J. Am. Chem. Soc.* **2008**, *130*, 5883–5885.
[20] H. Yang, J. Yan, Y. Wang, H. Su, L. Gell, X. Zhao, C. Xu, B. K. Teo, H. Häkkinen, N. Zheng, *J. Am. Chem. Soc.* **2017**, *139*, 31–34.
[21] H. Qian, W. T. Eckenhoff, Y. Zhu, T. Pintauer, R. Jin, *J. Am. Chem. Soc.* **2010**, *132*, 8280–8281.
[22] C. Zeng, H. Qian, T. Li, G. Li, N. L. Rosi, B. Yoon, R. N. Barnett, R. L. Whetten, U. Landman, R. Jin, *Angew. Chem. Int. Ed.* **2012**, *51*, 13114–13118.
[23] H. Yang, Y. Wang, H. Huang, L. Gell, L. Lehtovaara, S. Malola, H. Häkkinen, N. Zheng, *Nat. Commun.* **2013**, *4*, 2422.
[24] H. Yang, Y. Wang, N. Zheng, *Nanoscale* **2013**, *5*, 2674.
[25] H. Yang, Y. Wang, X. Chen, X. Zhao, L. Gu, H. Huang, J. Yan, C. Xu, G. Li, J. Wu, A. J. Edwards, B. Dittrich, Z. Tang, D. Wang, L. Lehtovaara, H. Häkkinen, N. Zheng, *Nat. Commun.* **2016**, *7*, 12809.
[26] A. Malinenko, A. Jonchère, L. Girard, S. Parrès-Maynadié, O. Diat, P. Bauduin, *Langmuir* **2018**, *34*, 2026–2038.
[27] T. Liu, *Langmuir* **2010**, *26*, 9202–9213.
[28] P. Kögerler, L. Cronin, *Angew. Chem. Int. Ed.* **2005**, *44*, 844–846.
[29] N. Yan, N. Xia, L. Liao, M. Zhu, F. Jin, R. Jin, Z. Wu, *Sci. Adv.* **2018**, *4*, eaat7259.
[30] T. Chen, Q. Yao, R. R. Nasaruddin, J. Xie, *Angew. Chem. Int. Ed.* **2019**, *58*, 11967–11977.
[31] R. P. Carney, J. Y. Kim, H. Qian, R. Jin, H. Mehenni, F. Stellacci, O. M. Bakr, *Nat. Commun.* **2011**, *2*, 335.
[32] L. Avram, Y. Cohen, *Chem. Soc. Rev.* **2015**, *44*, 586–602.
[33] S. Bestgen, O. Fuhr, B. Breitung, V. S. Kiran Chakravadhanula, G. Guthausen, F. Hennrich, W. Yu, M. M. Kappes, P. W. Roesky, D. Fenske, *Chem. Sci.* **2017**, *8*, 2235–2240.
[34] K. Salorinne, T. Lahtinen, J. Koivisto, E. Kalenius, M. Nissinen, M. Pettersson, H. Häkkinen, *Anal. Chem.* **2013**, *85*, 3489–3492.
[35] Z. Luo, Y. Yang, A. Radulescu, J. Kohlbrecher, T. A. Darwish, Q. K. Ong, S. Guldin, F. Stellacci, *Chem. Mater.* **2019**, *31*, 6750–6758.
[36] S. S. Berr, *J. Phys. Chem.* **1987**, *91*, 4760–4765.
[37] M. Hohenschutz, I. Grillo, O. Diat, P. Bauduin, *Angew. Chem. Int. Ed.* **2020**, *59*, 8084–8088.
[38] B. T. Diroll, K. M. Weigandt, D. Jishkariani, M. Cargnello, R. J. Murphy, L. A. Hough, C. B. Murray, B. Donnio, *Nano Lett.* **2015**, *15*, 8008–8012.
[39] M. Li, M. Zhang, Y. Lai, Y. Liu, C. Halbert, J. F. Browning, D. Liu, P. Yin, *J. Phys. Chem. C* **2020**, *124*, 15656–15662.
[40] Z. Luo, Y. Zhao, T. Darwish, Y. Wang, J. Hou, F. Stellacci, *Nat. Commun.* **2018**, *9*, 4478.
[41] Z. Luo, D. Marson, Q. K. Ong, A. Loiudice, J. Kohlbrecher, A. Radulescu, A. Krause-Heuer, T. Darwish, S. Balog, R. Buonsanti, D. I. Svergun, P. Posocco, F. Stellacci, *Nat. Commun.* **2018**, *9*, 1343.
[42] Q. Ong, Z. Luo, F. Stellacci, *Acc. Chem. Res.* **2017**, *50*, 1911–1919.
[43] Y. Lai, M. Li, M. Zhang, X. Li, J. Yuan, W. Wang, Q. Zhou, M. Huang, P. Yin, *Macromolecules* **2020**, *53*, 7178–7186.
[44] M. J. A. Hore, X. Ye, J. Ford, Y. Gao, J. Fei, Q. Wu, S. J. Rowan, R. J. Composto, C. B. Murray, B. Hammouda, *Nano Lett.* **2015**, *15*, 5730–5738.
[45] R. P. Rambo, J. A. Tainer, *Nature* **2013**, *496*, 477–481.
[46] D. I. Svergun, S. Richard, M. H. J. Koch, Z. Sayers, S. Kuprin, G. Zaccai, *Proc. Natl. Acad. Sci.* **1998**, *95*, 2267–2272.
[47] R. P. Rambo, J. A. Tainer, *Annu. Rev. Biophys.* **2013**, *42*, 415–441.

[48] M. P. Weir, D. T. W. Toolan, R. C. Kilbride, N. J. W. Penfold, A. L. Washington, S. M. King, J. Xiao, Z. Zhang, V. Gray, S. Dowland, J. Winkel, N. C. Greenham, R. H. Friend, A. Rao, A. J. Ryan, R. A. L. Jones, *J. Phys. Chem. Lett.* **2019**, *10*, 4713–4719.
[49] C. Kumara, X. Zuo, D. A. Cullen, A. Dass, *ACS Nano* **2014**, *8*, 6431–6439.
[50] M. Kotlarchyk, S. Chen, *J. Chem. Phys.* **1983**, *79*, 2461–2469.
[51] I. Breßler, J. Kohlbrecher, A. F. Thünemann, *J. Appl. Crystallogr.* **2015**, *48*, 1587–1598.
[52] C. A. Silvera Batista, R. G. Larson, N. A. Kotov, *Science* **2015**, *350*, 1242477.
[53] Q. Yao, Y. Yu, X. Yuan, Y. Yu, D. Zhao, J. Xie, J. Y. Lee, *Angew. Chem.* **2015**, *127*, 186–191.
[54] J. Yan, B. K. Teo, N. Zheng, *Acc. Chem. Res.* **2018**, *51*, 3084–3093.
[55] D. I. Svergun, *J. Appl. Crystallogr.* **1992**, *25*, 495–503.
[56] T. Higaki, C. Liu, M. Zhou, T.-Y. Luo, N. L. Rosi, R. Jin, *J. Am. Chem. Soc.* **2017**, *139*, 9994–10001.
[57] G. L. Hura, J. A. Tainer, *Nat. Biotechnol.* **2017**, *35*, 1044–1045.
[58] C. A. Brosey, J. A. Tainer, *Curr. Opin. Struct. Biol.* **2019**, *58*, 197–213.
[59] R. L. Pinals, D. Yang, D. J. Rosenberg, T. Chaudhary, A. R. Crothers, A. T. Iavarone, M. Hammel, M. P. Landry, *Angew. Chem. Int. Ed.* **2020**, *59*, 23668–23677.
[60] D. Franke, M. V. Petoukhov, P. V. Konarev, A. Panjkovich, A. Tuukkanen, H. D. T. Mertens, A. G. Kikhney, N. R. Hajizadeh, J. M. Franklin, C. M. Jeffries, D. I. Svergun, *J. Appl. Crystallogr.* **2017**, *50*, 1212–1225.

Entry for the Table of Contents

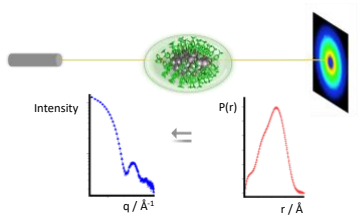

Small angle neutron scattering (SANS) can directly quantify the overall structure parameters of nanoclusters in solution. By adopting a core-shell ellipsoid model, the scattering patterns of a series of silver and gold nanoclusters can be correlated with their crystallographic structures. When combining with X-ray scattering, the molecular weight of both the metal core and the ligand shell can